J|A|C|S
ARTICLES
Published on Web 06/29/2002

Supramolecular Cation Assemblies of Hydrogen-Bonded (NH_4^+/$NH_2NH_3^+$)(Crown Ether) in [Ni(dmit)$_2$]-Based Molecular Conductors and Magnets

Tomoyuki Akutagawa,*,†,‡ Tatsuo Hasegawa,† Takayoshi Nakamura,*,† and Tamotsu Inabe§

Contribution from the Research Institute for Electronic Science, Hokkaido University, Sapporo 060-0812, Japan, PRESTO, Japan Science and Technology Corporation (JST), Japan, and Graduate School of Science, Hokkaido University, Sapporo 060-0810, Japan

Received March 15, 2002

Abstract: Hydrogen-bonded supramolecular cation assemblies of (NH_4^+/$NH_2-NH_3^+$)(crown ether), where the crown ether is [12]crown-4, [15]crown-5, or [18]crown-6, were incorporated into electrically conducting [Ni(dmit)$_2$] salts (dmit^{2-} = 2-thioxo-1,3-dithiole-4,5-dithiolate). (NH_4^+)([12]crown-4)[Ni(dmit)$_2$]$_3$(CH_3CN)$_2$ had a pyramidal shape, while ionic channels were observed in (NH_4^+)$_{0.88}$([15]crown-5)[Ni(dmit)$_2$]$_2$ and (NH_4^+)$_{0.70}$([18]crown-6)[Ni(dmit)$_2$]$_2$. Both (NH_4^+)$_{0.88}$([15]crown-5) and (NH_4^+)$_{0.70}$([18]crown-6) contained regularly spaced [Ni(dmit)$_2$] stacks formed by N−H···O hydrogen bonding between the oxygen atoms in crown ethers and the NH_4^+ ion. NH_4^+ occurred nonstoichiometrically; there were vacant ionic sites in the ionic channels. The ionic radius of NH_4^+ is larger than the cavity radius of [15]crown-5 and [18]crown-6. Therefore, NH_4^+ ions could not pass through the cavity and were distributed randomly in the ionic channels. The static disorder caused the conduction electrons to be randomly localized to the [Ni(dmit)$_2$] stacks. Hydrazinium ($NH_2-NH_3^+$) formed the supramolecular cations in ($NH_2-NH_3^+$)([12]crown-4)$_2$[Ni(dmit)$_2$]$_4$ and ($NH_2-NH_3^+$)$_2$([15]-crown-5)$_3$[Ni(dmit)$_2$]$_6$, possessing a sandwich and club-sandwich structure, respectively. To the best of our knowledge, these represent the first hydrazinium−crown ether assemblies to be identified in the solid. In the supramolecular cations, hydrogen bonding was detected between the ammonium or the amino protons of $NH_2-NH_3^+$ and the oxygen atoms of crown ethers. The sandwich-type cations coexisted with the [Ni(dmit)$_2$] dimer stacks. Although the assemblies were typically semiconducting, ferromagnetic interaction (Weiss temperature = +1 K) was detected in the case of ($NH_2-NH_3^+$)$_2$([15]crown-5)$_3$[Ni(dmit)$_2$]$_6$. The ($NH_2-NH_3^+$)$_{0.8}$([18]crown-6)[Ni(dmit)$_2$]$_2$ and (NH_4^+)$_{0.76}$([18]crown-6)[Ni(dmit)$_2$]$_2$ crystals were isomorphous. The large and flexible [18]crown-6 allowed for maintaining the same ionic channel structure through replacement of the NH_4^+ cation by $NH_2-NH_3^+$.

Introduction

Cation−crown ether complexes in the solid are formed through cation-binding atomic interactions between cations and the oxygen atoms of crown ethers. The complexes' structures depend on both the cation radius and the crown ether ring size.[1] The K^+ cation fits into the [18]crown-6 cavity, resulting in a typical planar (K^+)([18]crown-6) structure, while the K^+−[12]-crown-4 complex usually assumes a sandwich-type (K^+)([12]-crown-4)$_2$ structure. The strongest interaction between crown ethers and alkali cations occurs between the nucleophilic oxygen atoms in the crown ethers and the cations.[2] In addition to alkali cations, various types of ammonium cations, $R-NH_3^+$ (R = H, CH_3, $PhCH_2$, NH_2, etc.), have been known to form stable ammonium−crown ether complexes in the solid.[1] In these structures, the N−H$^+$···O hydrogen-bonding and electrostatic interactions both play an important role in binding the cations into the cavity of the crown ethers.[3] The ionic radius of NH_4^+ is the same as that of Rb^+ (1.48 Å), but slightly larger than that of K^+ (1.33 Å). The four H atoms in NH_4^+ are arranged in a tetrahedron around the central N atom. For a crown ether of a given ring size, the binding energies associated with Rb^+ and NH_4^+ are similar in solution.[4] The crystal structures of the inclusion compounds, however, are often quite different. In the solid, Rb^+ cation is usually coordinated to the oxygen atoms of crown ethers via isotropic electrostatic interactions, while the NH_4^+···O hydrogen bonds are aligned with the tetrahedral N−H hydrogen bonds. For example, the hydrogen bonds in (NH_4^+)([18]crown-6) were observed at the triangular C_3 oxygen

* To whom correspondence should be addressed. Phone: +81-11-706-2884. Fax: +81-11-706-4972. E-mail: takuta@imd.es.hokudai.ac.jp.
† Research Institute for Electronic Science, Hokkaido University.
‡ PRESTO, Japan Science and Technology Corporation.
§ Graduate School of Science, Hokkaido University.

(1) (a) Weber, E.; Toner, J. L.; Goldberg, I.; Vögtle, F.; Laidler, D. A.; Stoddart, J. F.; Bartsch, R. A.; Liotta, C. L. In *Crown Ethers and Analogues*; Patai, S., Rappoport, Z., Eds.; John Wiley & Sons: New York, 1989. (b) Gokel, G. W. In *Crown Ethers & Cryptands*; Stoddart, J. F., Ed.; RSC: Cambridge, 1994.
(2) Glendening, E. D.; Feller, D.; Thompson, M. A. *J. Am. Chem. Soc.* **1994**, *116*, 10657.
(3) Ha, Y. L.; Chakraborty, A. K. *J. Phys. Chem.* **1992**, *96*, 6410.
(4) (a) Izatt, R. M.; Bradshaw, J. S.; Nielsen, S. A.; Lamb, J. D.; Christensen, J. J.; Sen, D. *Chem. Rev.* **1985**, *85*, 271. (b) Izatt, R. M.; Pawlak, K.; Bradshaw, J. D.; Bruening, R. L. *Chem. Rev.* **1991**, *91*, 721.

Scheme 1. C_3 Hydrogen Bond

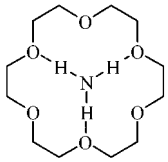

sites at the lower position of the [18]crown-6 O6-plane (Scheme 1).[5] Significant structural differences were observed between the sandwich-type $(Rb^+)([12]crown\text{-}4)_2$ and pyramidal-type $(NH_4^+)([12]crown\text{-}4)$ (Figure 1a and b).[6] The NH_4^+ ion was strongly coordinated to two oxygen atoms in [12]crown-4 and to two CH_3CN molecules, resulting in a tetrahedral $NH_4^+-(O2)_2(N2)_2$ coordination. By contrast, the isotropic Rb^+ ion was bound equally to eight oxygen atoms in two [12]crown-4 molecules located above and below the cation. Ammonium cations have the potential to form novel supramolecular cation assemblies by hydrogen bonding to crown ethers of varying size.

The two components of the hydrazinium ($NH_2-NH_3^+$) cation, the basic $-NH_2$ group and the cationic $-NH_3^+$, form sp^2- and sp^3-type hydrogen bonds, respectively. The crystal structure of $(NH_2-NH_3^+)([18]crown\text{-}6)(ClO_4^-)$ has been reported.[7] The $-NH_3^+$ site formed hydrogen bonds to three alternate C_3-oxygen sites of [18]crown-6, while the $-NH_2$ site formed hydrogen bonds with two oxygen atoms of ClO_4^- and three oxygen atoms of [18]crown-6 in the solid. This bifunctional molecular interaction has been utilized to form $NH_2-NH_3^+$ grafted layered assemblies of transition metal phosphates.[8] The basic $-NH_2$ site coordinates to transition metal ions, such as Fe^{2+}, Mn^{2+}, Co^{2+}, Ni^{2+}, and Cu^{2+}, while the $-NH_3^+$ site forms $N-H^+\cdots O$ hydrogen bonds with the phosphates layer.

We introduced supramolecular cation structures as counter-cations in $[Ni(dmit)_2]$ salts ($dmit^{2-}$ = 2-thioxo-1,3-dithiole-4,5-dithiolate).[9−11] This approach allows us to design the crystal structure of $[Ni(dmit)_2]$ salts with novel electrical and magnetic properties. In the case of conducting salts, the monovalent M^+-(crown ether) units were effective in modulating the $\pi-\pi$ stacking mode and lateral S−S interaction of the partially charge-transferred $[Ni(dmit)_2]^{-\delta}$ molecules.[9] The sandwich-type $(K^+)([12]crown\text{-}4)_2$ and planar, disc-shaped $K^+([18]crown\text{-}6)$ formed the $[Ni(dmit)_2]$ dimer and trimer molecules, respectively. Furthermore, the ionic channels, formed by regular arrays of

Scheme 2. $(NH_4^+/NH_2-NH_3^+)-(crown\ ethers)-[Ni(dmit)_2]$ System

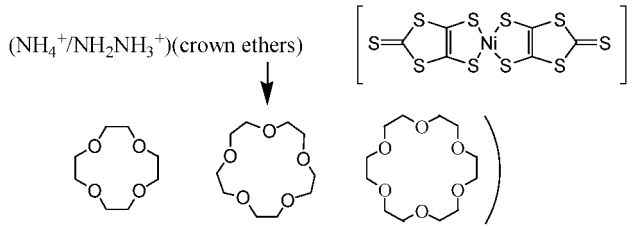

crown ethers, coexisted with the uniform, highly electrically conducting $[Ni(dmit)_2]$ stacks of $(Li^+)_{0.6}([15]crown\text{-}5)[Ni(dmit)_2]_2(H_2O)$ and $(M^+)_x([18]crown\text{-}6)[Ni(dmit)_2]_2$ ($M^+ = Li^+$, Na^+, and Cs^+).[10] For monovalent $[Ni(dmit)_2]$ salts, various types of supramolecular cations provided a large diversity of $S = {}^1/_2$ spin configuration according to the $[Ni(dmit)_2]^-$ anion arrangements.[11] Recently, we reported the formation of two-leg spin-ladder chains of $[Ni(dmit)_2]^-$ anions, induced by the hydrogen-bonded (anilinium)([18]crown-6) supramolecular structure.[12]

This report centers on supramolecular cation structures formed by the hydrogen bonding of NH_4^+ or $NH_2-NH_3^+$ to [12]crown-4, [15]crown-5, or [18]crown-6 in $[Ni(dmit)_2]$-based molecular conductors (Scheme 2). The hydrogen-bonding cations regulate the $[Ni(dmit)_2]$ configuration of electrically conducting salts. The structural, transport, and magnetic properties of five new salts, $(NH_4^+)_{0.88}([15]crown\text{-}5)[Ni(dmit)_2]_2$ (**1**), $(NH_4^+)_{0.70}([18]crown\text{-}6)[Ni(dmit)_2]_2$ (**2**), $(NH_2-NH_3^+)([12]crown\text{-}4)_2[Ni(dmit)_2]_4$ (**3**), $(NH_2-NH_3^+)_2([15]crown\text{-}5)_3[Ni(dmit)_2]_6$ (**4**), and $(NH_2-NH_3^+)_{0.8}([18]crown\text{-}6)[Ni(dmit)_2]_2$ (**5**), are compared with those of $(NH_4^+)([12]crown\text{-}4)[Ni(dmit)_2]_3(CH_3CN)_2$ (**6**), whose crystal structure and electrical properties were already reported,[6] and with those of the newly synthesized insulating salt $(NH_2-NH_3^+)([18]crown\text{-}6)[Ni(dmit)_2]$ (**7**). High electrical conductivity was observed in salts **1**−**6**, while the semiconducting salt **4** showed ferromagnetic interaction between the $[Ni(dmit)_2]$ molecules. Here we discuss the structural properties of the hydrogen-bonded supramolecular cations and the $[Ni(dmit)_2]$ configurations in terms of hydrogen-bonding geometries, intermolecular transfer integrals ($t \times 10^{-2}$ eV), electrical conductivities, and magnetic susceptibilities.

Experimental Section

Preparation of $[Ni(dmit)_2]$ Salts. Table 1 summarizes the crystal stoichiometry, shape, crystallization method, and solvent data for salts **1**−**7**. The precursor monovalent $(n\text{-}Bu_4N)[Ni(dmit)_2]$ salt was prepared according to the literature.[13] The crystals of salts **1**−**6** were grown using the standard electrocrystallization method in an *H*-shape cell (∼18 mL). The supporting electrolytes $(NH_4^+)(BF_4^-)$ and $(NH_2-NH_3^+)(BF_4^-)$ were recrystallized from CH_3CN or H_2O, and then dried in a vacuum. The electrocrystallization solvents CH_3CN and CH_3CN−acetone (1:1) were distilled prior to use. A constant current (1 μA) was applied to the platinum electrodes (1 mm ϕ) for 2 weeks at room temperature. The stoichiometry of crystals **1**−**4** was determined by X-ray structural and elemental analyses. Salt **5** was obtained in polycrystalline form; thus the stoichiometry of $(NH_2-NH_3^+)_{0.8}([18]crown\text{-}6)[Ni(dmit)_2]_2$ was determined using elemental analysis ($C_{24}H_{28}N_{1.6}O_6S_{20}Ni_2$ found C, 23.79; H, 2.27; N, 1.99; calc C, 24.15; H, 2.35; N, 1.88). The monovalent salt, $(NH_2-NH_3^+)([18]crown\text{-}6)[Ni(dmit)_2]$ (**7**), was prepared in CH_3CN applying the diffusion method to $(n\text{-}Bu_4N)[Ni(dmit)_2]$ and $(NH_2-NH_3^+)(BF_4^-)$.

(5) Nagao, O.; Kobayashi, A.; Sasaki, Y. *Bull. Chem. Soc. Jpn*. **1978**, *51*, 790.
(6) Akutagawa, T.; Hasegawa, T.; Nakamura, T.; Takeda, S.; Inabe, T.; Sugiura, K.; Sakata, Y.; Underhill, A. E. *Inorg. Chem*. **2000**, *39*, 2645.
(7) Trueblood, K. N.; Knobler, C. B.; Lawrence, D. S.; Stevens, R. V. *J. Am. Chem. Soc*. **1982**, *104*, 1355.
(8) Ekambaram, S.; Sevov, S. C. *J. Mater. Chem*. **2000**, *10*, 2522.
(9) (a) Akutagawa, T.; Nakamura, T.; Inabe, T.; Underhill, A. E. *J. Mater. Chem*. **1996**, *7*, 135. (b) Akutagawa, T.; Nakamura, T.; Inabe, T.; Underhill, A. E. *Thin Solid Films* **1998**, *331*, 264. (c) Akutagawa, T.; Nakamura, T. *Coord. Chem. Rev*. **2000**, *198*, 297. (d) Akutagawa, T.; Nezu, Y.; Hasegawa, T.; Nakamura, T.; Sugiura, K.; Sakata, Y.; Inabe, T.; Underhill, A. E. *Chem. Commun*. **1998**, 2599. (e) Robertson, N.; Akutagawa, T.; Nakamura, T.; Roehrs, S.; Underhill, A. E. *J. Mater. Chem*. **1999**, *9*, 1233. (f) Akutagawa, T.; Hasegawa, T.; Nakamura, T.; Inabe, T.; Sugiura, K.; Sakata, Y.; Underhill, A. E. *Synth. Met*. **1999**, *102*, 1747.
(10) (a) Nakamura, T.; Akutagawa, T.; Honda, K.; Underhill, A. E.; Coomber, A. T.; Friend, R. H. *Nature* **1998**, *394*, 159. (b) Akutagawa, T.; Hasegawa, T.; Nakamura, T.; Takeda, S.; Inabe, T.; Sugiura, K.; Sakata, Y.; Underhill, A. E. *Chem.-Eur. J*. **2001**, *7*, 4902.
(11) (a) Takamatsu, N.; Akutagawa, T.; Hasegawa, T.; Nakamura, T.; Inabe, T.; Fujita, W.; Awaga, K. *Inorg. Chem*. **2000**, *39*, 870. (b) Akutagawa, T.; Nishihara, S.; Takamatsu, N.; Hasegawa, T.; Nakamura, T.; Inabe, T. *J. Phys. Chem. B* **2000**, *104*, 5871. (c) Akutagawa, T.; Takamatsu, N.; Shitagami; Hasegawa, T.; Nakamura, T.; Inabe, T. *J. Mater. Chem*. **2001**, *11*, 2118.
(12) Nishihara, S.; Akutagawa, T.; Hasegawa, T.; Nakamura, T. *Chem. Commun*. **2002**, 408.

Table 1. Crystal Stoichiometry, Shape, and Crystallization Solvent Data of Salts **1**−**7**

entry	stoichiometry	shape	method	solvent
1	$(NH_4^+)_{0.88}$([15]crown-5)[Ni(dmit)$_2$]$_2$	needle	electrocrystallization	CH_3CN
2	$(NH_4^+)_{0.70}$([18]crown-6)[Ni(dmit)$_2$]$_2$	needle	electrocrystallization	CH_3CN−acetone[b]
3	$(NH_2-NH_3^+)$([12]crown-4)$_2$[Ni(dmit)$_2$]$_4$	plate	electrocrystallization	CH_3CN
4	$(NH_2-NH_3^+)_2$([15]crown-5)$_3$[Ni(dmit)$_2$]$_6$	plate	electrocrystallization	CH_3CN
5	$(NH_2-NH_3^+)_{0.8}$([18]crown-6)[Ni(dmit)$_2$]$_2$[c]	plate	electrocrystallization	CH_3CN
6[a]	(NH_4^+)([12]crown-4)[Ni(dmit)$_2$]$_3$$(CH_3CN)_2$	plate	electrocrystallization	CH_3CN
7	$(NH_2-NH_3^+)$([18]crown-6)[Ni(dmit)$_2$]	block	diffusion	CH_3CN

[a] Reference 6. [b] CH_3CN:acetone = 1:1. [c] Stoichiometry based on elemental analysis.

Table 2. Crystallographic Data of Salts **1**−**4** and **7**

	1	**2**	**3**	**4**	**7**
formula	$C_{22}H_{24}N_{0.9}O_5S_{20}Ni_2$	$C_{24}H_{27}N_{0.7}O_6S_{20}Ni_2$	$C_{20}H_{19}NO_4S_{20}Ni_2$	$C_{33}H_{35}N_2O_{7.5}S_{30}Ni_3$	$C_{18}H_{29}N_2O_6S_{10}Ni$
fw	1139.27	1179.77	1095.55	1717.70	748.80
crystal system	monoclinic	monoclinic	orthorhombic	triclinic	triclinic
space group	$P2_1$ (No. 4)	$P2_1/n$ (No. 14)	$P2_12_12$ (No. 18)	$P\bar{1}$ (No. 2)	$P\bar{1}$ (No. 2)
crystal size, mm^3	0.5 × 0.1 × 0.05	0.6 × 0.05 × 0.05	0.7 × 0.2 × 0.1	0.6 × 0.2 × 0.1	0.7 × 0.3 × 0.1
a, Å	4.3997(1)	4.5583(6)	11.5998(9)	8.127(1)	10.4795(9)
b, Å	21.6237(8)	11.318(1)	41.943(3)	16.9556(3)	12.6141(9)
c, Å	21.4816(8)	42.825(6)	7.8620(4)	21.9281(9)	12.714(1)
α, deg				89.531(1)	68.2(2)
β, deg	92.488(1)	92.11(1)		86.901(2)	82.791(4)
γ, deg				79.845(3)	80.221(3)
V, Å^3	2041.8(1)	2207.8(4)	3825.1(4)	2970.0(3)	1534.1(1)
Z	2	2	4	2	2
D_{calc}, g cm^{-3}	1.852	1.800	1.931	1.920	1.610
temperature, K	296	296	296	100	296
μ, cm^{-1}	19.81	18.37	21.11	20.44	13.49
no. of reflections measured	4776	5954	4107	12 730	14 231
no. of independent reflections	4764	5081	4081	10 185	6918
no. of reflections used	2638	2682	2225	8275	5229
R[a]	0.046	0.058	0.038	0.050	0.039
R_w[a]	0.086	0.075	0.066	0.077	0.037
GOF	1.07	1.16	1.16	0.86	1.28

[a] $R = \sum||F_o| - |F_c||/\sum|F_o|$ and $R_w = [\sum(\omega(F_o^2 - F_c^2)^2)/\sum\omega(F_o^2)^2]^{1/2}$.

Crystal Structure Determination. Crystallographic data (Table 2) were collected by a Rigaku AFC-5R or Raxis-Rapid diffractometer using Mo Kα (λ = 0.71073 Å) radiation from a graphite monochromator. Structure refinements were performed by the full-matrix least-squares method on F^2. Calculations were performed using Crystal Structure software packages.[14] Parameters were refined using anisotropic temperature factors except for the [15]crown-5 in salt **1** and the hydrogen atom. The large thermal motion of [15]crown-5 in salt **1** prevented the application of anisotropic thermal parameters. [15]crown-5 was assumed to have a disordered configuration in salt **4**, whose hydrogen atoms were not excluded from the refinements. The $NH_2-NH_3^+$ cation exhibited orientational disorder in salt **4**; the occupancy factors of two orientations were determined to be 0.7 and 0.3 per crown ether. The refined occupancy factor for the NH_4^+ ion in salts **1** and **2** was found to be 0.88 and 0.70, respectively.

Electrical Conductivity. The temperature-dependent electrical conductivity was measured by the dc four-probe method along the long axis of the crystal. The stacking direction of the [Ni(dmit)$_2$] molecules was aligned with the long axis of the crystal. Electrical contacts were prepared using gold paste to attach 10 μm ϕ gold wires to the crystals (Tokuriki 8560).

Magnetic Susceptibility. The temperature-dependent magnetic susceptibility was measured by a SQUID magnetometer (Quantum Design Model MPMS-5) for polycrystalline samples. The applied magnetic field was 1 T for all measurements.

Calculation of Transfer Integrals. The transfer integrals (t) were calculated within the tight-binding approximation using the extended Hückel molecular orbital method. The LUMO of the [Ni(dmit)$_2$] molecule was used as the basis function.[15] The semiempirical parameters for Slater-type atomic orbitals were taken from ref 15. The t value between each pair of molecules was assumed to be proportional to the overlap integral (S) via the equation $t = -10S$ eV.

Results and Discussion

Crystals of $(NH_4^+)_{0.88}$([15]crown-5)[Ni(dmit)$_2$]$_2$ (**1**) and $(NH_4^+)_{0.70}$([18]crown-6)[Ni(dmit)$_2$]$_2$ (**2**) were composed of cationic $(NH_4^+)_x$(crown ether) supramolecules and fractionally charged [Ni(dmit)$_2$]$^{-\delta}$ molecules. The degree of charge transfer (δ) on each [Ni(dmit)$_2$] molecule in salts **1** and **2** was 0.44 and 0.35 electrons, respectively. The supramolecular cation formed ionic channels, in stark contrast to the pyramidal structure of (NH_4^+)([12]crown-4)$_2$[Ni(dmit)$_2$]$_4$$(CH_3CN)_2$ (**6**). Replacing the NH_4^+ with $NH_2-NH_3^+$ yielded the electrically conducting salts $(NH_2-NH_3^+)$([12]crown-4)$_2$[Ni(dmit)$_2$]$_4$ (**3**), $(NH_2-NH_3^+)_2$([15]crown-5)$_3$[Ni(dmit)$_2$]$_6$ (**4**), and $(NH_2-NH_3^+)_{0.8}$([18]crown-6)[Ni(dmit)$_2$]$_2$ (**5**). The crystal structures of salts **3** and **4** differed

(13) Steinmecke, G.; Sieler, H. J.; Krimes, R.; Hoyer, E. *Phosphorus Sulfur* **1979**, *7*, 49.
(14) Crystal Structure: Single-crystal structure analysis software. Ver. 1.0, 2000. Rigaku Corporation and Molecular Structure Corporation. For ortep drawing: Farrugia, L. J. *J. Appl. Crystallogr.* **1997**, *32*, 565.
(15) Mori, T.; Kobayashi, A.; Sasaki, Y.; Kobayashi, H.; Saito, G.; Inokuchi, H. *Bull. Chem. Soc. Jpn.* **1984**, *57*, 627.

Table 3. Hydrogen-Bonding Parameters of Salts **1**−**4**, **6**, and **7**

entry	ammonium N–H$^+$–O, Å	amine N–H–O, Å	NH_2–S or N–N, Å
1	O1−N1 = 3.22(4), O1−N1 = 3.29(4) O2−N1 = 3.85(3), O2−N1 = 2.96(3) O3−N1 = 3.15(4), O3−N1 = 3.35(4) O4−N1 = 3.40(4), O4−N1 = 3.26(4) O5−N1 = 3.50(3), O5−N1 = 3.14(3)		
2	O1−N1 = 3.15(2), O1−N1 = 2.91(1) O2−N1 = 2.99(1), O2−N1 = 3.06(1) O3−N1 = 3.08(1), O3−N1 = 2.89(1)		N1−N1 = 2.30(3) N1−N1 = 2.38(3)
3	O1−N1 = 3.24(2) O2−N1 = 3.12(2) O3−N1 = 3.01(2) O4−N1 = 2.88(1)	O1−N2 = 3.10(2) O2−N2 = 3.46(2) O4−N2 = 3.67(2)	S13−N2 = 3.579(7)
4	O1−N1 = 2.825(9), O6−N4 = 2.77(2) O2−N1 = 2.855(8), O7−N4 = 2.94(2) O3−N1 = 3.343(9), O8−N4 = 2.55(2) O4−N1 = 3.13(1), O9−N4 = 2.55(2) O5−N1 = 2.755(8), O10−N4 = 2.60(2)	O4−N2 = 2.89(1) O6−N3 = 3.04(2) O7−N3 = 3.16(2) O8−N3 = 3.24(2)	S28−N3 = 3.16(1) S28−N2 = 3.66(1)
6	O1−N1= 2.92(1) O2−N1 = 2.85(1)		N1−N2 = 3.02(2)
7	O1−N1 = 2.89(1) O2−N1 = 2.99(2) O3−N1 = 2.833(3) O4−N1 = 2.93(2) O5−N1 = 2.87(2) O6−N1 = 2.91(2)	S1−N2 = 3.71(6) S2−N2 = 3.83(8)	S1−N2 = 3.70(6) S2−N2 = 3.82(8) S1−N2 = 3.86(4)

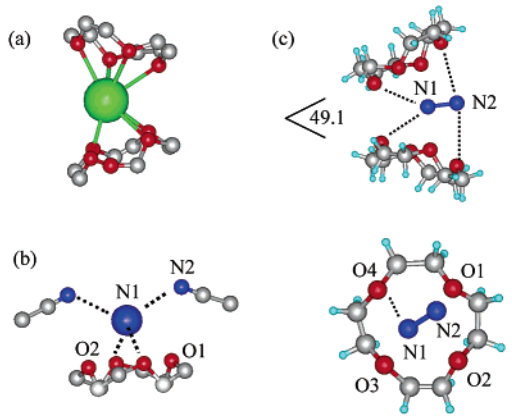

Figure 1. Supramolecular cation structures of (M^+)([12]crown-4). (a) Sandwich cation structure in $(Rb^+)([12]crown\text{-}4)_2[Ni(dmit)_2]_4$. (b) Pyramidal $(NH_4^+)([12]crown\text{-}4)(CH_3CN)_2$ structure in salt **6**. (c) Sandwich $(NH_2-NH_3^+)([12]crown\text{-}4)_2$ structure in salt **3**, viewed parallel (above) and normal (below) to the [12]crown-4 plane. The dashed lines show the effective hydrogen-bonding interactions.

from those of salts **6** and **1**, while salt **5** was isomorphous with salt **2** with respect to lattice parameter. The δ on each [Ni(dmit)$_2$] molecule for salts **3**, **4**, and **5** is 0.25, 0.33, and 0.4.

Supramolecular Cation Structures. The (NH_4^+)(crown ether) cations in salts **1** and **2** were ionic channel type supramolecules of $[(NH_4^+)_{0.88}([15]crown\text{-}5)]_\infty$ and $[(NH_4^+)_{0.70}([18]crown\text{-}6)]_\infty$, respectively. As reported previously,[6] the supramolecular cation in salt **6** had a pyramidal structure, and the NH_4^+ ion was strongly coordinated to two oxygen atoms of [12]crown-4 (N1−O1 = 2.85(1) Å). The other N1−O2 distance of 2.92(1) Å was roughly 0.1 Å longer than the N1−O1 distance (Figure 1b). The NH_4^+ ion is tetrahedrally coordinated to the nitrogen atoms of two CH_3CN molecules and $(O1)_2$. The N1−N2 distance was 3.02(2) Å. Although the ionic radius of NH_4^+ is the same as that of Rb^+, the configuration of [12]crown-4 molecules around the Rb^+ ion was notably different (Figure 1a). The hydrogen-bonding parameters are tabulated in Table 3.

$(NH_2-NH_3^+)([12]crown\text{-}4)_2$. The supramolecular cations in salt **3** resemble the sandwich-type structures of $(M^+)([12]crown\text{-}4)_2$ in the $(M^+)([12]crown\text{-}4)_2[Ni(dmit)_2]_4$ salts (M^+ = Na^+, K^+, and Rb^+). The rodlike $NH_2-NH_3^+$ cation was sandwiched by two [12]crown-4 molecules (Figure 1c). The mean oxygen plane of two [12]crown-4 molecules in salt **3** formed an angle θ = 49.1°, which was larger than those for $(Na^+)([12]crown\text{-}4)_2$ (θ = 0°), $(K^+)([12]crown\text{-}4)_2$ (θ = 29.5°), and $(Rb^+)([12]crown\text{-}4)_2$ (θ = 35.1°).[6] The increase in cation size from Rb^+ to $NH_2-NH_3^+$ enhanced the distortion angle of the sandwich coordination. The inclusion ability of crown ethers is considered to be much higher at the cationic $-NH_3^+$ site than at the neutral $-NH_2$ site.[1] The NH_3^+ site is located at the center of the $([12]crown\text{-}4)_2$ sandwich unit.

N−H$^+$···O type hydrogen bonds between eight oxygen atoms of [12]crown-4 and the NH_3^+ site were observed. The N1−O4 distance of 2.88(1) Å is within the range of the standard N−O hydrogen bond distance (2.87 Å).[16] The second shortest was the O3−N1 distance (3.01(2) Å). Two N1−O4 hydrogen bonds mainly connect the NH_3^+ moiety between two [12]crown-4. In addition, a weak atomic interaction between the amino protons and the oxygen atoms of [12]crown-4 was observed at a N2−O1 distance of 3.10(2) Å.

$[(NH_4^+)_{0.88}([15]crown\text{-}5)]_\infty$. Ionic channels were observed through the regular stacks of $(NH_4^+)_{0.88}([15]crown\text{-}5)$ in salt **1**. Figure 2a shows the ionic channel structure of salt **1** viewed parallel and perpendicular to the [15]crown-5 plane. Because the ionic radius of NH_4^+ (1.46 Å) is larger than the cavity radius of [15]crown-5, NH_4^+ ions are located at the inversion centers between two [15]crown-5 planes. The distance between NH_4^+ and the mean O5-plane of [15]crown-5 is 2.341 Å. NH_3^+ ion is coordinated to 10 oxygen atoms in two [15]crown-5, one located above, one below. The average N−O hydrogen bond length of 3.31 Å is, however, significantly larger than the standard N−O hydrogen bond length (2.87 Å).[16] This type of

(16) Jeffrey, G. A. In *An Introduction to Hydrogen Bonding*; Truhlar, D. G., Ed.; Oxford University Press: New York, 1997.

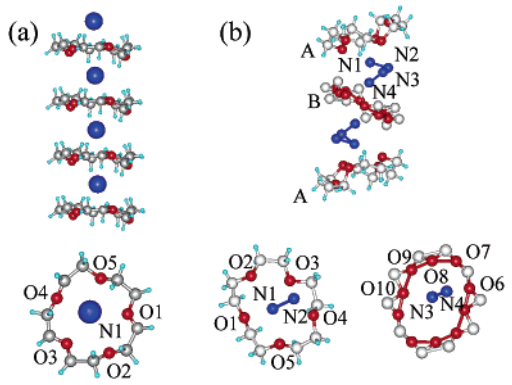

Figure 2. Supramolecular cation structures in salts **1** and **4**. (a) Ionic channels through uniform $(NH_4^+)_{0.88}$([15]crown-5) stacks in salt **1**. (b) Club-sandwich $(NH_2{-}NH_3^+)_2$([15]crown-5)$_3$ structure in salt **4**. Orientational disorder is observed in the central [15]crown-5 **B** and $NH_2{-}NH_3^+$ (N1−N2 and N3−N4).

ionic channel structure has been observed in the $(Cs^+)_{0.8}$([18]-crown-6)[Ni(dmit)$_2$]$_2$ salt, in which Cs^+ ions were located between two [18]crown-6 planes. The ionic channels of salt **1** had vacant ionic sites within the channel, whose occupancy factor was 0.88. X-ray diffuse scattering at 100 K detected no superstructure associated with a periodic arrangement of NH_4^+, suggesting a random distribution of the NH_4^+ ions.

$(NH_2{-}NH_3^+)_2$([15]crown-5)$_3$. The cation $(NH_2{-}NH_3^+)_2$([15]-crown-5)$_3$ in salt **4** had a club-sandwich structure. A similar structure was observed for $(Cs^+)_2$([18]crown-6)$_3$.[17] The crystallographically asymmetric cation structure was composed of one $NH_2{-}NH_3^+$, one [15]crown-5 **A** unit, and one-half of a [15]crown-5 **B** unit (Figure 2b). Because of the inversion center located on the [15]crown-5 **B**, molecule **B** had two orientations. The molecular planes **A** and **B** formed an angle of 52°, resulting in a largely deformed club-sandwich cation structure. Orientational disorder of the $NH_2{-}NH_3^+$ cation was observed in the form of N1−N2 and N3−N4 configurations, with occupancy factors of 0.7 and 0.3, respectively. In the N1−N2 orientation, the three N−O hydrogen bond lengths N1−O1 = 2.825(9), N1−O2 = 2.855(8), and N1−O3 = 2.755(8) Å were all shorter than the standard N−H$^+$···O hydrogen bond length.[16] In addition, an N2−O4 interaction between the amino proton and an oxygen atom was observed at a distance of 2.89(1) Å. The disordered **B** molecule was observed to be tightly coordinated to the $-NH_3^+$ site in the N3−N4 orientation. The N−O distances in the **B** molecule were shorter than the standard N−O hydrogen bond length. Three NH_2−O interactions occurred between the N3 and the O6, O7, and O8 atoms at 3.04(2), 3.16(2), and 3.24-(2) Å, respectively. The ammonium N1 and N4 sites were located 1.798 and 1.671 Å above the [15]crown-5 **A** and **B** planes, respectively.

$[(NH_4^+)_{0.70}$([18]crown-6)$]_\infty$. The ionic channel structure through the regular stack of $(NH_4^+)_{0.70}$([18]crown-6) in salt **2** was oriented along the *a*-axis (Figure 3a). Two NH_4^+ sites located 1.15 Å above and below the mean O6-plane of [18]-crown-6 were related via an inversion center. The nearest neighboring N−N distances of 2.30(3) and 2.38(3) Å were too short to occupy these ionic sites simultaneously. The average N−O hydrogen-bonding distance of 3.03 Å was longer than the standard N−H$^+$···O hydrogen bond.[16] The mean interplanar

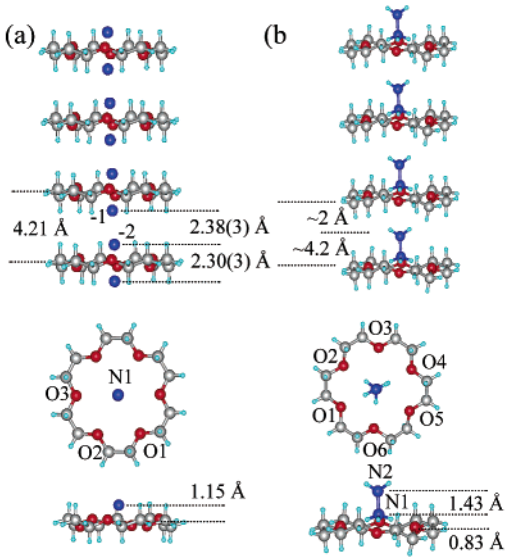

Figure 3. Supramolecular cation structures in salts **2**, **5**, and **7**. (a) Ionic channels through $(NH_4^+)_{0.7}$([18]crown-6) stacks in salt **2**. Two NH_4^+ sites (−1 and −2) are related via the inversion center. (b) $(NH_2{-}NH_3^+)$([18]-crown-6) structure in salt **7** (below) and predicted ionic channel structure of $(NH_2{-}NH_3^+)_{0.8}$([18]crown-6) in salt **5** (above).

distance between the O6-planes of [18]crown-6 along the *a*-axis was 4.21 Å. The Li^+ ion in the isostructural salt $(Li^+)_x$([18]-crown-6)[Ni(dmit)$_2$]$_2$ had a motional freedom through the [18]-crown-6 cavity.[10b] Replacing Li^+ with Na^+ or Cs^+ changed the system from a dynamic to a static disordered state. The ionic channels of salt **2** contained vacant ionic sites; the channels' occupancy factor was 0.70. Because the ionic radius of NH_4^+ is larger than that of Na^+, it can be safely concluded that the two disordered NH_4^+ sites in salt **2** had a static character.

$[(NH_2{-}NH_3^+)_{0.80}$([18]crown-6)$]_\infty$. We predict the $(NH_2{-}NH_3^+)$([18]crown-6) cation's crystal structure in salt **5** on the basis of salt **7**, and its stacking structure on the basis of salt **2**. The lattice parameters of salt **5** (a = 4.42, b = 11.42, c = 42.95 Å, β = 89.3°) were virtually the same as those of salt **2**. Hence, we assumed salt **5** crystals to be isomorphous with those of salt **2**. The electrical conductivity and magnetic susceptibility measurements were consistent with the assumed structure (see below). Figure 3b shows the cation structure of $(NH_2{-}NH_3^+)$-([18]crown-6) in salt **7**. As expected, the $-NH_3^+$ site was coordinated to six oxygen atoms of [18]crown-6 with an average N−O distance of 2.90 Å, well in the range of the standard NH_4^+···O hydrogen-bonding distance.[16] The N1 and N2 atoms were located 0.83 and 2.26 Å above the mean O_6-plane of [18]crown-6, respectively. The $-NH_3^+$ site in salt **7** penetrated much further into the cavity of [18]crown-6 than that in salt **2**. The N1−N2 bond was almost normal to the mean O6-plane of [18]crown-6 (91.75°).

The local hydrogen-bonding structure of $(NH_2{-}NH_3^+)$([18]-crown-6) was expected to be the same as that in salt **5**. The lattice parameters of salts **2** and **5** along the *a*-axis were 4.56 and 4.42 Å, respectively, which suggests a similar stacking distance for the [18]crown-6 planes along this axis. The ionic channel structure of salt **5** can be assumed to be as illustrated in Figure 3b, with an interplanar distance of 4.2 Å. The distance between the $-NH_2$ site and upper mean O6-plane of [18]crown-6 was estimated to be 2 Å, that is, long enough to allow the $(NH_2{-}NH_3^+)$([18]crown-6) stacking structure along the *a*-axis.

(17) Vidal, J. L.; Schoening, R. C.; Troup, J. M. *Inorg. Chem.* **1981**, *20*, 227.

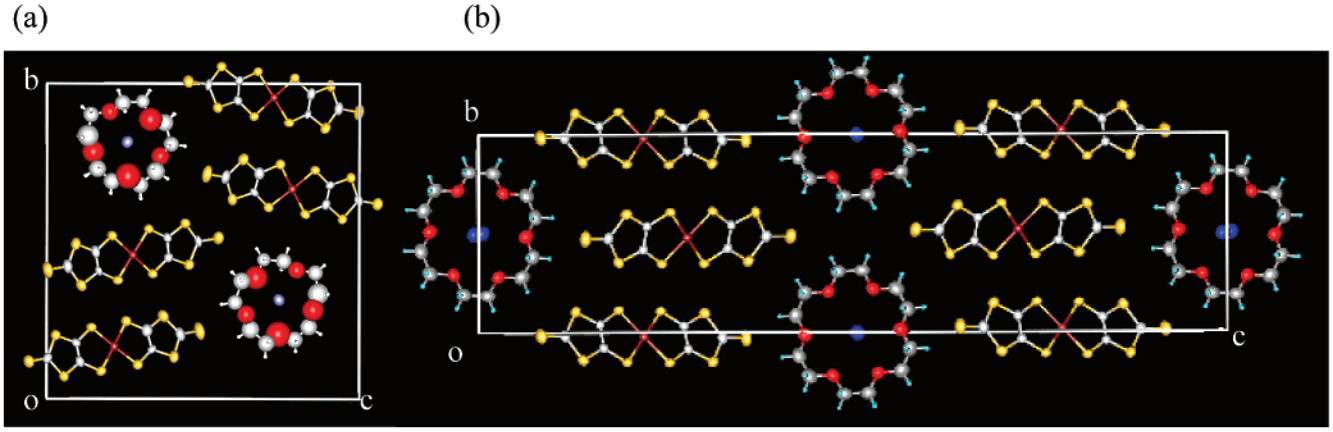

Figure 4. Crystal structures of salts **1** and **2**. Unit cell of salts **1** (a) and **2** (b), as viewed along the *a*-axis.

Table 4. Transfer Integrals *t* for [Ni(dmit)$_2$] Configuration[a]

transfer integral (10^{-2} eV)	1	2	3	4
t_1 (t_1')	12.66	12.27	−18.74	−16.42 (14.70)
t_2 (t_2')	1.21	−0.83	4.70	−0.19 (0.73)
t_3 (t_3')	−0.5	0.25	1.4	−0.73 (−0.06)
t_4 (t_4')			1.05	0.24 (0.72)
t_5 (t_5')			1.82	0.42 (0.20)
t_6 (t_6')			1.24	0.34 (0.10)

[a] Transfer integrals were calculated from the LUMO of [Ni(dmit)$_2$] on the basis of the extended Hückel calculation ($t = -10S$ eV; S is the overlap integral).

On the basis of the stoichiometry of $(NH_2{-}NH_3^+)_{0.8}$([18]crown-6)[Ni(dmit)$_2$]$_2$, there should be vacant ionic sites in the ionic channel.

[Ni(dmit)$_2$] Configurations. The electrical conductivity properties are directly related to the molecular interaction modes of [Ni(dmit)$_2$] molecules in the crystals. We predict the [Ni(dmit)$_2$] configuration on the basis of the transfer integrals ($t \times 10^{-2}$ eV). Table 4 tabulates the transfer integrals for salts **1**−**4**.

Salt **6** crystals were composed of nonuniform trimer stacks of [Ni(dmit)$_2$]$^{-0.33}$, which in turn formed the layered structure through lateral S−S contacts.[6] The (NH_4^+)([12]crown-4) cations were located in the interlayer spaces between the electrically conducting [Ni(dmit)$_2$] layers.

The crystal structures of salts **1** and **2** were isomorphous with $(Li^+)_{0.6}$([15]crown-5)[Ni(dmit)$_2$]$_2$(H_2O) and $(Li^+)_x$([18]crown-6)[Ni(dmit)$_2$]$_2$, respectively.[10] The [Ni(dmit)$_2$] formed regular stacks along the *a*-axis, that is, parallel to the ionic channel structures in salts **1** and **2**. The difference in ionic channel diameter between $[(NH_4^+)_{0.88}$([15]crown-5)$]_\infty$ and $[(NH_4^+)_{0.70}$([18]crown-6)$]_\infty$ was reflected by the different packing arrangements of [Ni(dmit)$_2$] stacks and ionic channels. Figure 4a and b shows the unit cell of salts **1** and **2**, respectively, as viewed along the *a*-axis. In salt **1**, two uniform [Ni(dmit)$_2$] stacks interacted via the lateral S−S contacts along the *b*-axis, forming the two-leg ladder structure. By contrast, infinite lateral S−S contacts were observed in salt **2** along the *b*-axis. The ionic channel of salt **1** was surrounded by four [Ni(dmit)$_2$] ladders, while that of salt **2** lied in the *ab*-plane.

The intrastack interactions along the *a*-axis in salts **1** and **2** fell within the same order of magnitude: $t_1 = 12.7$ and 12.27, respectively. The lateral interaction ($t_2 = 1.21$) along the *b*-axis of salt **1** is ca. 10 times smaller than that along the *a*-axis.

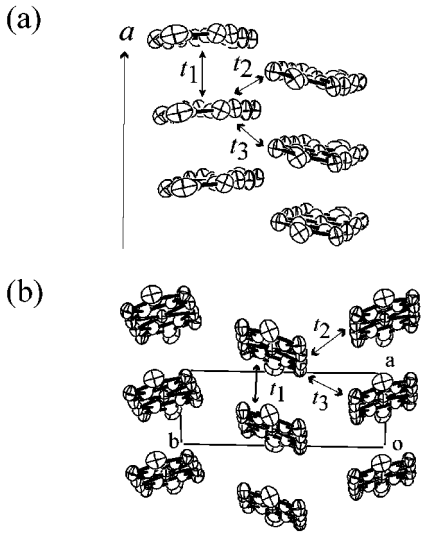

Figure 5. [Ni(dmit)$_2$] arrangements and band structures of salts **1** (a) and **2** (b); the intermolecular interactions in [Ni(dmit)$_2$] stacks viewed along the long axis.

Furthermore, the interstack interaction ($t_3 = -0.5$) observed between the [Ni(dmit)$_2$] ladders along the ($b + c$)-direction is quite weak. The three-dimensional molecular interactions along the *a*-, *b*-, and ($b + c$)-axes observed in salt **1** were insufficient to increase the dimensionality of the electronic structure. The lateral interstack interactions ($t_2 = -0.83$, $t_3 = 0.25$) in salt **2** are quite weak, and also insufficient to increase the electronic dimensionality. An alternate arrangement of [Ni(dmit)$_2$] layers and ionic channels along the *c*-axis completely suppresses the interlayer interaction of [Ni(dmit)$_2$] along this *c*-axis (Figure 5).

The replacement of NH_4^+ by $NH_2{-}NH_3^+$ in salt **3** transformed the supramolecular cationic structure from the pyramidal to the sandwich structure, which in turn altered the [Ni(dmit)$_2$] stacking structure from nonuniform trimers to dimer stacks. Two kinds of [Ni(dmit)$_2$] (**A** and **B**) were present in salt **3**. Figure 6a and b shows the unit cell of salt **3** viewed along the *c*- and *b*-axes, respectively. Salt **3** crystals were virtually isomorphous with (M^+)([12]crown-4)$_2$[Ni(dmit)$_2$]$_4$ (M^+ = Na^+, K^+, and Rb^+).[6] The [Ni(dmit)$_2$] stacks were arranged along the *a*-axis through lateral S−S interactions, forming an electrically conducting [Ni(dmit)$_2$] layer within the *ac*-plane. The supramolecular cations were located in the interlayer spaces. The S13

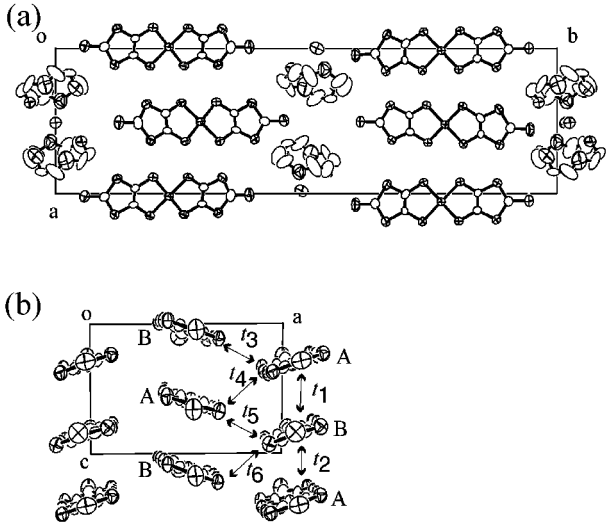

Figure 6. Crystal structure of salt **3**. Unit cell viewed along the *c*-axis (a) and along the *b*-axis (b). **A** and **B** correspond to the crystallographically asymmetric [Ni(dmit)$_2$] species. Intermolecular interaction modes in the *ac*-plane, along with transfer integrals (t_1-t_6) are shown.

terminal sulfur and the N2 amino proton interacted weakly at a distance of 3.579(7) Å.

The **A**−**B** dimers, the fundamental structural units within the stacks, are stacked along the *c*-axis. The intradimer interaction **A**−**B** ($t_1 = -18.74$) is ca. 4 times stronger than the interdimer interaction ($t_2 = 4.70$). The lateral S−S interactions of the [Ni(dmit)$_2$] stacks along the $2a + c$ ($t_3 = 1.4$ and $t_5 = 1.8$) and $-2a + c$ ($t_4 = 1.1$ and $t_6 = 1.2$) directions are considerably weak as compared to the intrastack interactions (Figure 6b).

The club-sandwich structure of the $(NH_2-NH_3^+)_2$([15]crown-5)$_3$ cation yielded [Ni(dmit)$_2$] dimer stacks. The substitution of NH_4^+ with the only slightly different $NH_2-NH_3^+$ ion clearly induced a significant change in the [Ni(dmit)$_2$] configuration. Figure 7a and b shows the salt **4** unit cell viewed along the *c*- and *b*-axes, respectively. Three kinds of [Ni(dmit)$_2$] (**A**, **B**, and **C**) were observed in salt **4**. The [Ni(dmit)$_2$] stacks lied along the *a*-axis bound together via lateral S−S contacts, forming the layered [Ni(dmit)$_2$] structure within the *ac*-plane. The supramolecular cations were located within the interlayer spaces, exhibiting two weak interactions between the S28 terminal sulfur and the N2 and N3 amino protons, at 3.66(1) and 3.16(7) Å, respectively.

The [Ni(dmit)$_2$] layers were composed of two kinds of stacks, −(**A**−**B**)− and −(**C**−**C**)−, both oriented along the *c*-axis. The fundamental **A**−**B** ($t_1 = -16.4$) and **C**−**C** ($t_1' = 14.7$) dimer units have strong intradimer interactions. In both stacks, the interdimer interactions $t_2 = -0.19$ and $t_2' = 0.73$ are considerably smaller than the intradimer interactions. Eight kinds of weak lateral S−S interactions with *t* values of less than about 1 were observed along the $3a + c$ (t_3, t_5, t_4', and t_6') and $3a - c$ (t_4, t_6, t_3', and t_5) directions within the *ac*-plane. The electronic state of salt **5** was predominated by the two kinds of isolated [Ni(dmit)$_2$] dimers.

Because it is isomorphous with salt **2**, salt **5** was expected to have the same [Ni(dmit)$_2$] stacking structure and one-dimensional electronic structure as those of salt **2**.

Electrical Conductivity and Magnetic Susceptibility. The electrical and magnetic properties were mainly determined by the [Ni(dmit)$_2$] configuration in the crystals. The transfer integral

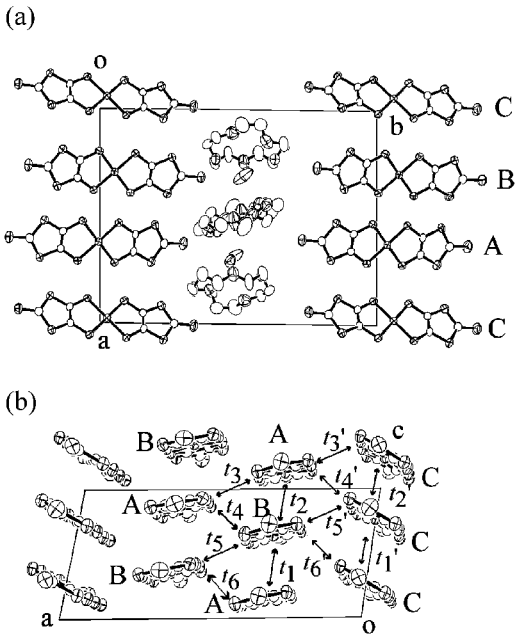

Figure 7. Crystal structure of salt **4**. Unit cell viewed along the *c*-axis (a) and along the *b*-axis (b). **A**, **B**, and **C** are crystallographically asymmetric [Ni(dmit)$_2$] species. The intermolecular interaction mode in the *ac*-plane and transfer integrals (t_1-t_6') are illustrated.

Table 5. Electrical Conductivities at Room Temperature (σ_{RT}), Activation Energy (E_a), and Magnetic Behavior of Salts **1**−**6**

entry	σ_{RT}[a] S cm^{-1}	E_a eV	magnetic behavior[b]	magnetic parameter[b]
1	16.0	0.026[c]	DAH	$\gamma = 0.35$
2	3.0	0.02[c]	DAH	$\gamma = 0.18$
3	0.2	0.20	Curie	$C = 0.37$
4	0.5	0.20	Curie−Weiss	$C = 0.75$ ($\theta = +1$ K)
5	35.0	0.02[c]	DAH	$\gamma = 0.20$
6	0.14	0.140	Curie	$C = 0.31$

[a] Measured by the standard four-probe dc method. [b] DAH is the disordered Heisenberg antiferromagnetic model, which is fitted by $\chi_{mol} \propto 1/T^{1-\gamma}$. Parameters C, γ, and θ are the Curie constant, γ in DAH equation, and Weiss temperature, respectively. [c] Determined at the temperature range above 100 K.

calculation yielded similar one-dimensional electronic structures for salts **1** and **2**. We first discuss the electrical and magnetic properties of these two salts, as well as salt **5**, which is expected to have the same [Ni(dmit)$_2$] stacking structure as salt **2**. Table 5 summarizes electrical conductivities at room temperature (σ_{RT}, S cm^{-1}), activation energy (E_a, eV), and magnetic behavior of salts **1**−**6**.

The room-temperature electrical conductivities of salts **1**, **2**, and **5** were 16.0, 3.0, and 35.0 S cm^{-1}, respectively. Figure 8a shows the temperature-dependent electrical resistivities normalized by the room-temperature values (ρ/ρ_{300K}). The inset is an expansion in the temperature range from 150 to 300 K. In contrast to our expectations, resistivity measurements revealed salts **1**, **2**, and **5** to possess semiconducting, rather than metallic, properties. The activation energies of salts **1**, **2**, and **5** above 100 K are rather low: 0.026, 0.020, and 0.020 eV, respectively. A resistivity hump was detected for salt **5** at around 50 K. The preliminary study detected a dielectric anomaly at that temperature. High electrical conductivity, however, prevented precise evaluation of the dielectric properties of salt **5**.[18]

Figure 8b shows the temperature-dependent molar magnetic susceptibility (χ_{mol}) of salts **1**, **2**, and **5**. χ_{mol} was observed to

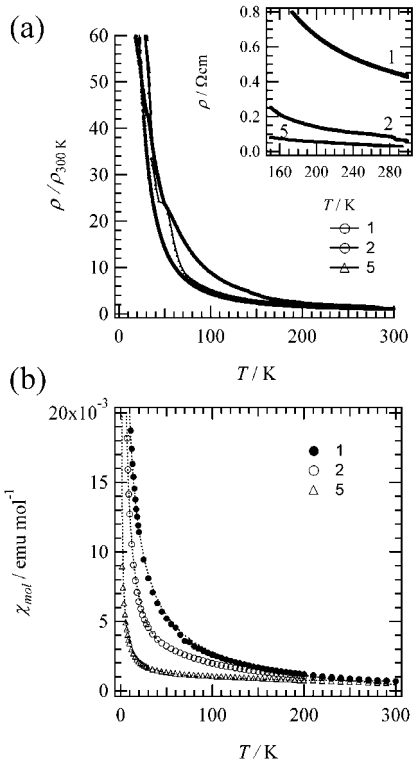

Figure 8. Electrical and magnetic behavior of salts **1**, **2**, and **5**. (a) Temperature-dependent electrical resistivity normalized with respect to the values at 300 K (ρ/ρ_{300K}). The inset is an expansion in the temperature range from 150 to 300 K. (b) Temperature-dependent magnetic susceptibility (χ_m) of salts **1** (○), **2** (●), and **5** (△). Dashed lines are the fits obtained through the disordered Heisenberg antiferromagnetic model (see text).

increase monotonically with decreasing temperature below 200 K. The magnetic behavior suggested by these data did not agree with the metallic electronic state. In the previous section, we established the static disorder of NH_4^+ and $NH_2-NH_3^+$ cations in the ionic channel. The NH_4^+ and $NH_2-NH_3^+$ ions in salts **1**, **2**, and **5** are nonstoichiometric and randomly distributed between the ionic sites. The static disorders of the cation species should have influenced the conduction electrons on the evenly spaced [Ni(dmit)$_2$] stacks, especially for those with a one-dimensional electronic structure. Thus, we employed the disordered antiferromagnetic Heisenberg model to account for the temperature-dependent magnetic susceptibilities.[19] The model is based on a probability distribution of the magnetic exchange energy J in random magnetic interaction and uses a canonical transformation to reduce the temperature dependence of χ_{mol} to $\chi_{mol} \propto 1/T^{1-\gamma}$. The $\chi_{mol}-T$ behavior of salts **1**, **2**, and **5** could be fitted via this model using $\gamma = 0.35$, 0.18, and 0.20, respectively.

The random distribution of the NH_4^+ and $NH_2-NH_3^+$ within the ionic channels generated a static random potential field in the crystal lattice, which acted as a pinning potential for conduction electrons within the one-dimensional [Ni(dmit)$_2$] electronic structure.[20] This localized the spins on the [Ni(dmit)$_2$] stacks despite the high electrical conductivities. The randomly occupied spins on regular [Ni(dmit)$_2$] stacks induced the probability distribution of magnetic interaction J, leading us to

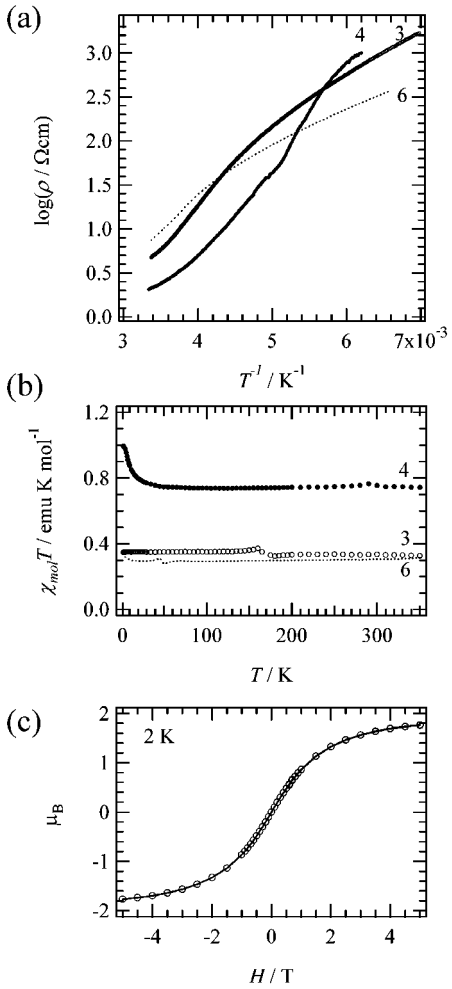

Figure 9. Electrical and magnetic behavior of salts **3**, **4**, and **6**. (a) Logarithmic resistivity (log ρ/Ω cm) vs inverse of temperature (T^{-1}/K^{-1}). (b) $\chi_{mol}T$ vs T plots for salts **3**, **4**, and **6**. Solid line in salt **4** represents results predicted by the Curie−Weiss law. (c) Magnetization (M, μ_B) vs magnetic field (H) for salt **4** at 2 K.

the conclusion that salts **1**, **2**, and **5** were in the semiconductor because of the static disorder of the NH_4^+ and $NH_2-NH_3^+$ cations in their ionic channels.

Salts **3** and **4** had nonuniform [Ni(dmit)$_2$] dimer stacks, which were expected to be semiconducting. The room-temperature electrical conductivities of salts **3** and **4** were 0.2 and 0.5 S cm^{-1}, respectively. Figure 9a shows the logarithmic plots of resistivity versus the inverse of temperature (log $\rho-T$) for salts **3** and **4**, along with salt **6**. The activation energies of salts **3**, **4**, and **6** were 0.2, 0.2, and 0.14 eV ($T > 200$ K), respectively, 1 order of magnitude higher than those of salts **1**, **2**, and **5**. Electrical conduction in salts **3** and **4** predominantly occurred by thermally activated hopping processes between the strongly dimerized [Ni(dmit)$_2$] stacks. Lowering the temperature completely localized the conduction electrons lacking thermal excitation to the [Ni(dmit)$_2$] sites, which exhibited a localized magnetic spin behavior.

χ_m values increased monotonically with decreasing temperature in salts **3** and **4**. Figure 9b shows the $\chi_{mol}T$ versus T plots of salts **3**, **4**, and **6**. On the basis of the stoichiometries of these salts, we expected one $S = {}^1/_2$ spin per formula unit for salts **3** and **6** and two $S = {}^1/_2$ spins per formula unit for salt **4**. In salts **3** and **6**, $\chi_{mol}T$ was virtually independent of temperature over

(18) Akutagawa, T., unpublished results.
(19) (a) Theodorou, G.; Cohen, M. H. *Phys. Rev. Lett.* **1976**, *37*, 1014. (b) Theodorou, G. *Phys. Rev. B* **1977**, *16*, 2273.
(20) Mott, N. F. *Metal−Insulator Transition*, 2nd ed.; Taylor & Francis: 1990.

the entire measured range, and the Curie constants were consistent with one $S = {}^1/_2$ spin of $C = 0.37$ emu K mol^{-1}.

Salt **4** exhibited ferromagnetic interaction below 20 K. Its magnetization above 20 K was consistent with two $S = {}^1/_2$ spins of $C = 0.75$ emu K mol^{-1}. Below 20 K, the increase of the $\chi_m T$ (Weiss temperature $\theta = +1$) indicated ferromagnetic behavior. The $\chi_{mol} T$ value reached 1.0 emu K mol^{-1} at 2 K. The magnetization curve ($M-H$) over the range of applied magnetic field from -5 to 5 T (2 K) was nonlinear, which is typical of ferromagnetic systems.[21] The magnetic moment (μ_B) saturated toward $2\mu_B$ with increasing magnetic field, which was consistent given the two $S = {}^1/_2$ spin contributions of [Ni(dmit)$_2$]. However, no hysteresis was observed in the $M-H$ curve at 2 K.

Ferromagnetic interaction in [Fe(Me$_5$C$_5$)$_2$][Ni(dmit)$_2$] and ferromagnetic ordering in [Mn(Me$_5$C$_5$)$_2$][Ni(dmit)$_2$] below 2.5 K have been reported.[22] The charge-transfer excitation between the donor [Fe(Me$_5$C$_5$)$_2$] and acceptor [Ni(dmit)$_2$]$^-$ has been identified as the origin of the ferromagnetic interaction in these salts. In salt **4**, the ferromagnetic interaction results from the [Ni(dmit)$_2$] arrangement itself because the countercations have a closed-shell electronic structure. The magnetic spin exchange between the monovalent [Ni(dmit)$_2$]$^-$ anions is usually observed to be antiferromagnetic. We have reported a variety of [Ni(dmit)$_2$]$^-$ anion arrangements through the application of the supramolecular cation approach. The magnetism of these salts ranges from a one-dimensional antiferromagnetic linear Heisenberg chain to singlet−triplet thermal excitation in dimers, and two-leg spin-ladder associated with the face-to-face π-stacking and lateral S−S contacts of the monovalent [Ni(dmit)$_2$]$^-$ anions in the crystal.[11,12] In all cases, antiferromagnetic spin interactions between the [Ni(dmit)$_2$]$^-$ anions were predominant.

In the partially charge-transferred [Ni(dmit)$_2$]$^{-0.33}$ state of salt **4**, the neutral [Ni(dmit)$_2$]^0 and monovalent [Ni(dmit)$_2$]$^-$ anion species coexisted. Such low-temperature charge ordering states render possible ferromagnetic spin interaction between [Ni(dmit)$_2$]$^-$ anions via the neutral [Ni(dmit)$_2$]^0. The superexchange interaction through the empty LUMO orbitals of neutral [Ni(dmit)$_2$]^0 molecules results in the ferromagnetic interaction between the [Ni(dmit)$_2$]$^-$ anions. To the best of our knowledge, salt **4** is the first example of a partially charge-transferred [Ni(dmit)$_2$] salt showing ferromagnetic coupling.

Conclusions

Supramolecular cation structures of (NH_4^+)(crown ethers) and ($NH_2-NH_3^+$)(crown ethers) were incorporated into partially charge-transferred electrically conducting [Ni(dmit)$_2$] salts. Hydrogen-bonding interactions between the ammonium and the oxygen atoms in the crown ethers were confirmed. The (NH_4^+)([12]crown-4) in (NH_4^+)([12]crown-4)[Ni(dmit)$_2$]$_3$(CH$_3$CN)$_2$ exhibited a pyramidal structure, whereas [15]crown-5 and [18]crown-6 formed ionic channel structures in (NH_4^+)$_{0.88}$([15]crown-5)[Ni(dmit)$_2$]$_2$ and (NH_4^+)$_{0.70}$([18]crown-6)[Ni(dmit)$_2$]$_2$. Although considerably weak as compared to standard N−O hydrogen bonds, the hydrogen-bonding interactions within the ionic channels were sufficient to provide the driving force for the construction of regular arrays of crown ethers. The NH_4^+ ions, distributed randomly within the ionic channels, acted as pinning potentials for conduction electrons, rendering the salts semiconducting, despite the regular stacks of [Ni(dmit)$_2$]. The magnetic properties, which corresponded to a disordered metallic state, were explained by the disordered Heisenberg antiferromagnetic chain model.

The $NH_2-NH_3^+$ yielded sandwich ($NH_2-NH_3^+$)([12]crown-4)$_2$ and club-sandwich ($NH_2-NH_3^+$)$_2$([15]crown-5)$_3$ structures. These supramolecular cation structures were basically constructed by the N−H$^+$···O hydrogen-bonding interactions between the oxygen atoms of crown ethers and the ammonium moiety of hydrazinium. Similar hydrogen-bonding interactions were observed between oxygen atoms of crown ethers and amino protons. The ($NH_2-NH_3^+$)([12]crown-4)$_2$[Ni(dmit)$_2$]$_4$ had a [Ni(dmit)$_2$] dimer structure, which exhibited a semiconducting and localized magnetic spin behavior. The ($NH_2-NH_3^+$)$_{0.8}$([18]crown-6)[Ni(dmit)$_2$]$_2$ was found to be isomorphous with (NH_4^+)$_{0.7}$([18]crown-6)[Ni(dmit)$_2$]$_2$. Finally, ($NH_2-NH_3^+$)([15]crown-5)$_3$[Ni(dmit)$_2$]$_6$ exhibited a ferromagnetic interaction (Weiss temperature $= +1$ K). To the best of our knowledge, this represents the first example of a [Ni(dmit)$_2$] salt showing ferromagnetic coupling in the absence of a magnetic cation. The supramolecular cation approach is useful for constructing various types of [Ni(dmit)$_2$] configuration in the crystal. Further designs of hydrogen-bonded supramolecular cations containing organic ammonium are now in progress to fabricate novel [Ni(dmit)$_2$]-based molecular conductors and magnets.

Acknowledgment. This work was partly supported by a Grant-in-Aid for Science Research from the Ministries of Education, Culture, Sports, Science, and Technology of Japan. The authors would like to thank Dr. M. Wakeshima and Prof. Y. Hinatsu for allowing the use of their SQUID magnetometer.

Supporting Information Available: Atomic coordinates, anisotropic thermal parameters, bond lengths for crystals **1**−**4**, and crystal structure of **7** (PDF). This material is available free of charge via the Internet at http://pubs.acs.org.

JA026211G

(21) Miller, J. S.; Epstein, A. J. *Angew. Chem., Int. Ed. Engl.* **1994**, *33*, 385.
(22) (a) Broderick, W. E.; Thompson, J. A.; Godfrey, M. R.; Sabat, M.; Hoffman, B. M. *J. Am. Chem. Soc.* **1989**, *111*, 7657. (b) Faulmann, F.; Pullen, A. E.; Riviere, E.; Journaux, Y.; Retailleau, L.; Cassoux, P. *Synth. Met.* **1999**, *103*, 2296.